Impact of hydrodynamics on effective interactions in suspensions of active and passive matter

Ryan C. Krafnick and Angel E. García

Phys. Rev. E **91**, 022308 — Published 19 February 2015

DOI: 10.1103/PhysRevE.91.022308

Impact of Hydrodynamics on Effective Interactions in Suspensions of Active and Passive Matter

Ryan C. Krafnick* and Angel E. García†
Department of Physics, Applied Physics, and Astronomy, Rensselaer Polytechnic Institute, Troy, NY 12180, USA.

Passive particles exhibit unique properties when immersed in an active bath of self-propelling entities. In particular, an effective attraction can appear between particles that repel each other when in a passive solution. Here we numerically study the effect of hydrodynamics on an active-passive hybrid system, where we observe qualitative differences as compared to simulations with excluded volume effects alone. The results shed light on an existing discrepancy in pair lifetimes between simulation and experiment, due to the hydrodynamically enhanced stability of coupled passive particles.

PACS numbers: 82.70.Dd, 87.17.Jj, 47.15.G-

Introduction.—Active, self-propelling entities are ubiquitous in biological and physical systems, comprising suspensions of bacteria [1–5], eukaryotes [6], manufactured nanomotors [7–9], zooplankton [10], and algae [11] to name a few. These nonequilibrium systems exhibit intriguing collective behaviours such as self-assembly [12], phase separation [13], and coherent, coordinated motions [2–4, 14]. The presence of active matter also causes unique properties to appear in suspensions of passive particles, including enhanced diffusion (effective temperature) [6, 15–18] and pair formation (effective interactions) [19]. Improving our understanding of the complex behaviors of these systems and the interplay between active and passive bodies is vital to their application to such problems as the targeted delivery of microscopic cargos [20], the development of micromotors [21] and shuttles [22], nanometer-scale mixing [23], and water remediation [24].

As an active body propels itself through a medium, it creates a fluid flow that extends toward other objects, facilitating both short and long range interactions [25, 26]. For example, the bacterium *Escherichia coli* produces a dipole flow field as it swims (see Fig. 1), with fluid being forced out the front and back of its trajectory by its head and flagella respectively. The role of these hydrodynamic effects in various forms of emergent behavior is, however, a central, unresolved issue in the field of active matter, with the impact being characterized as anywhere from neglible and quantitative [21] to pivotal and qualitative [27, 28]. This variation demonstrates the importance in determining how hydrodynamic interactions influence each emergent property of a system.

When passive colloidal particles are immersed along with active particles, the off-equilibrium driving force of the active matter leads to an effective attraction between the passive elements [19]. The active matter in this case can be seen as a fluctuating field around the passive particles, where forces aligned along a pair's connecting line tend to reduce the separation between the particles. The role of hydrodynamics on the stability and dynamics of the resulting pairs, however, remains unknown, as previously the work in Ref. [19] evaluated only steric forces between particles. While excluded volume collisions between particles can lead to pair formation, certain aspects of the fluid flow (e.g., the entrainment of fluid perpendicular to a bacterium's trajectory) cause directional behavior impossible to realize with steric interactions alone.

In this Letter, we computationally analyze the impact of hydrodynamics on the diffusion and pair formation of passive particles embedded in an active bacterial suspension. The active bodies are run-and-tumble particles (representing *E. coli*) while the passive entities are spheres (representing latex beads). Run-and-tumble dynamics (exhibited by some bacteria) cycles between a period of straight propulsion at constant velocity v followed by a (much shorter) period of tumbling, in which the orientation of the object is randomized. This allows the bacterium to explore its environment in a random walk pattern over long time scales. While directly related to the motion of certain bacteria, this model can also be mapped [29] onto active Brownian particles such as self-phoretic Janus spheres [13, 30, 31]; therefore, the results can be extended to a variety of systems beyond simple run-and-tumble dynamics. We find that the presence of explicit hydrodynamics enhances the pair stability of passive particles, evident in the shift of a peak in the radial distribution function. Furthermore, the degree of coordination and number of contacts is substantially increased in simulations with hydrodynamics. We note that this study concerns only so-called pushers, which are the class of swimmers relevant to the referenced literature, and does not examine the dynamics of pullers [26].

Method.—We simulate N_p passive spheres of diameter d and N_a active rods of length l (along the swim direction) and width w in a 2D box of side length L. Typical experiments are quasi-2D [16, 19], and the effective free-slip 3rd dimension in simulations is comparable to,

* krafnr@rpi.edu
† angel@rpi.edu

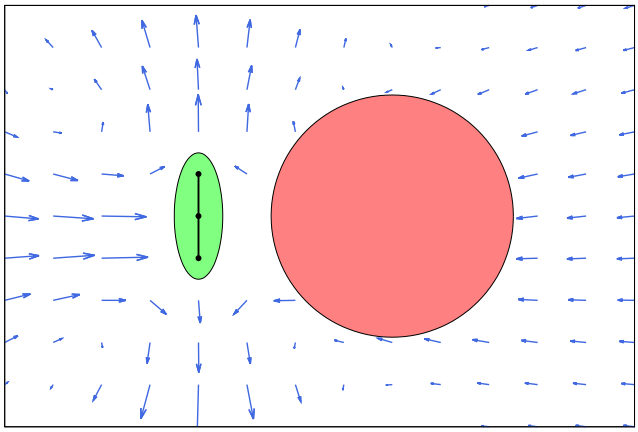

FIG. 1. (color online). Fluid flow around a swimmer (green) alongside a passive particle (red). Blue vectors indicate the velocity of the fluid at each location, and the swimming direction is directly downward. The force centers of the swimmer are also shown (black circles). The distance between field vectors is 1 µm.

e.g., a suspended soap film [16]. A rod can be in either the run or tumble phase (denoted with boolean θ, where $\theta = 0$ and $\theta = 1$ correspond to run and tumble phases respectively), with characteristic durations τ_r and τ_t respectively (transitions between phases occur with rate $1/\tau_r$ and $1/\tau_t$). The rods have an orientation unit vector $\hat{\mathbf{e}}$ and have $C = 3$ force centers aligned with it (see Fig. 1). Given a position $\mathbf{r}$, these centers are located at $\mathbf{r}$ and $\mathbf{r} \pm \hat{\mathbf{e}}l/3$ (the rods considered have a length to width ratio of $l/w = 3$, suitable for *E. coli* [16]). Direct interaction between particles is due to a pairwise excluded volume force $\mathbf{f}_E$ between force centers, given by

$$\mathbf{f}_E(\mathbf{r}_i^p, \mathbf{r}_j^q) = A\, max(a_i + a_j - |\mathbf{r}_i^p - \mathbf{r}_j^q|, 0), \qquad (1)$$

where a_i is the radius ($w/2$ for a rod) of the ith particle and $\mathbf{r}_i^p$ is the location of the pth force center of the ith particle. A determines the magnitude, which is set high enough to prevent appreciable overlap. For simulations that include hydrodynamics, the fluid velocity field is modelled via the lattice Boltzmann method [32], which allows for a simple and powerful coupling of fluid and particle dynamics via the immersed boundary method [33] and has previously been adapted to active matter simulations [34, 35]. In this method, the fluid-particle force $\mathbf{f}_F$ takes place via a friction term evaluated at a series of nodes across the particle's surface, and takes the form

$$\mathbf{f}_F(\mathbf{r}_i^j) = \gamma_i(\mathbf{u}(\mathbf{r}_i^j) - \mathbf{v}_i^j), \qquad (2)$$

where $\mathbf{r}_i^j$ is the position of node j, γ_i is the friction coefficient, $\mathbf{u}$ is the (interpolated) fluid velocity, and $\mathbf{v}_i^j$ is the velocity of the particle at node j. A force equal in magnitude but opposite in direction is applied back onto the fluid at each node, such that the total momentum of the system is conserved. Brownian dynamics is neglected in the present study because the velocity of active matter is orders of magnitude larger than that created by thermal fluctuations, which would place a needless restriction on the timestep. The active nature of the bath is the primary cause of the dynamics [19] in contrast to thermal depletion effects [36]. A rod experiences a self-propulsion force $\mathbf{f}_R = B\,\hat{\mathbf{e}}(1 - \theta_i)$ (with an equal and opposite force applied to the fluid) and a zero-mean, Gaussian distributed random torque $\mathbf{T}_R = \xi_R\theta_i$. The variance of this torque determines the average rate of change in orientation during a tumbling event. The self-propulsion magnitude B determines the maximum swimming speed. The total force and torque on rod i are thus

$$\begin{aligned}\mathbf{F}_i &= \sum_j^{S_i} \mathbf{f}_F(\mathbf{r}_i^j) + \sum_{j\neq i}^{N_a+N_p} \sum_{p,q}^{C_i,C_j} \mathbf{f}_E(\mathbf{r}_i^p, \mathbf{r}_j^q) + \mathbf{f}_R, \\ \mathbf{T}_i &= \sum_j^{S_i} (\mathbf{r}_i^j - \mathbf{r}_i) \times \mathbf{f}_F(\mathbf{r}_i^j) + \sum_p^{C_i} (\mathbf{r}_i^p - \mathbf{r}_i) \times \mathbf{f}_E^p + \mathbf{T}_R,\end{aligned} \qquad (3)$$

where the ith particle has S_i surface nodes and $\mathbf{f}_E^p$ is the sum of the excluded volume forces on force center p. These equations are integrated using a modified leapfrog algorithm (since the force depends on velocity), given by

$$\begin{aligned}\mathbf{v}(t + \Delta t) &= \frac{\mathbf{F}\Delta t/m}{1 + \gamma\Delta t/2m} + \frac{1 - \gamma\Delta t/2m}{1 + \gamma\Delta t/2m}\mathbf{v}(t), \\ \mathbf{r}(t + 3\Delta t/2) &= \mathbf{r}(t + \Delta t/2) + \mathbf{v}(t + \Delta t)\Delta t,\end{aligned} \qquad (4)$$

with particle mass m, where the term $\mathbf{F}$ does not include the $\mathbf{v}$ component of the friction, for clarity. This equation follows from assuming the friction acts on the average velocity of a particle during the time interval Δt. These equations mainly serve to smooth out the momentum transfer with the fluid lattice, as the motion of particles inevitably reduces to

$$\mathbf{v} = \mathbf{F}/\gamma, \qquad (5)$$

due to the low Reynolds number (low velocity, high viscosity—no memory) of the system.

We simulate spheres of diameter $d = 5$ µm, and rods of $l = 3$ µm and $w = 1$ µm. The self-propulsion magnitude B is fixed such that the swimmers achieve a velocity of 30 µm/s (i.e., $B/\gamma = v$). The variance of ξ_R (the tumbling torque) is set to be consistent with the experimentally observed average change in orientation of *E. coli* during a tumbling event (around 68°, see Table 1 of [37]), which is sufficient to prevent any long term correlation in swimmer orientation. Here $\langle \xi_R(t)\xi_R(t')\rangle = 4k_BT\gamma\delta(t - t')$, where γ is the swimmer friction coefficient, k_B is Boltzmann's constant, and T is the temperature (300 K). This form was chosen to correspond to the thermal fluctuations seen in Brownian Dynamics (BD), but there is no temperature in these simulations. Friction coefficients take the general form $\gamma = \phi\rho\nu d$ where ϕ is a

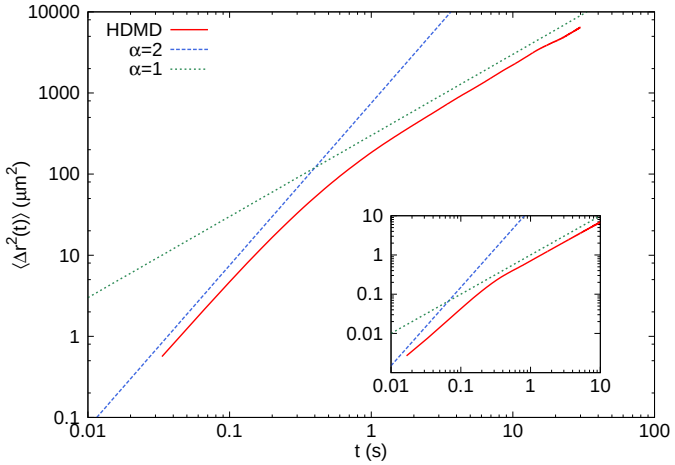

FIG. 2. (color online). Mean squared displacement of the HDMD (red solid) simulation as a function of time, with ($\Delta r^2 \propto t^\alpha$) ballistic (blue dashed) and simple diffusive (green dotted) curves also shown. At short times the spheres exhibit superdiffusive motion, owing to correlated interactions with the swimmer fluid flows and collisions, but this eventually transitions into simple diffusion for t >1 s (due to reduced correlation). Inset: same plot for MD simulations, where the same characteristics can be seen, but the shift occurs on a shorter timescale, at a much lower magnitude.

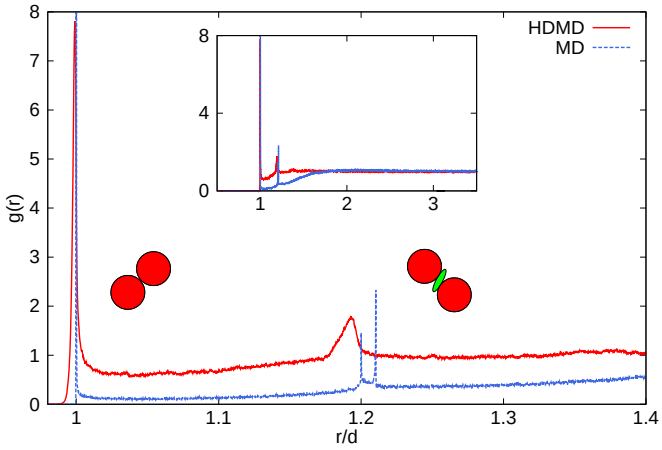

FIG. 3. (color online). Radial distribution function $g(r)$ for HDMD (red solid) and MD (blue dashed) simulations, with the distance in units of sphere diameter d. Adjacent graphics indicate the typical formation leading to the shown peaks. MD peaks are narrow due to the relatively low rate of collisions for a close pair. It takes a long time for particles to get knocked out of the tightly bound state, and they are generally pushed directly out to the secondary peaks upon splitting. The two separate MD peaks at $1.2d$ are due to different angles and local rod formations when a swimmer splits a pair, and the distinction is not significant. Inset: same plot zoomed out to see the full range.

constant, ρ is the fluid density (1000 kg/m^3 for water), and ν is the kinematic viscosity (10^{-6} m^2/s for water). We choose $\phi_{sphere} = 16/3$ (suitable for a disk), and $\phi_{rod} = 1.27\phi_{sphere}$ (where the prefactor comes from the aspect ratio). Different schemes of choosing ϕ tend to yield the same order of magnitude, and different values were not found to significantly impact the results (consider that the swimming speed will remain unchanged, so the value of ϕ mainly affects the value of B). The box length $L = 128$ μm was chosen to reduce the error in the fluid velocity field around a swimmer (caused by periodic boundary conditions) below 5%. We set $N_p = 33$ and $N_a = 330$, which corresponds to a coverage of 10% of the area. Data for 60 simulations with hydrodynamics and (mechanical) molecular dynamics (hereafter referred to as HDMD) with timestep 1/6 μs and run time 28 s and 60 simulations with molecular dynamics alone (hereafter referred to as MD) with timestep 1/6 x 10^2 μs and run time 60 minutes were collected. The MD simulations still have a friction force, but there is no fluid velocity field. This distinction allows us to elucidate the contribution of explicit hydrodynamics to the problem. The difference in timestep comes from the need to propagate the fluid field across the lattice at a suitable speed, but the MD simulations progress very slowly in comparison to the HDMD runs (as will be discussed below) such that the two run times are comparable dynamically.

Results.—The mean squared displacement (MSD) of spheres in HDMD simulations is given in Fig. 2 as a function of time. Spheres exhibit superdiffusive (near ballistic) motion at short time scales, due to the driving motion of nearby swimmers (which increases velocity correlation from one time to the next). At long timescales the spheres transition into a simple diffusive motion, since the field of swimmers leads to random impulses (a well-known result, see [16] for example). The timescale of the transition from superdiffusive to simple diffusive motion is comparable to the typical duration of a swimmer's run period. This can be interpreted as the time scale of constant-direction force being applied to a particle, prior to the onset of random impulses. The inset of Fig. 2 also gives the diffusion for MD simulations, which shows a similar behavior; however, the transition occurs at a shorter timescale and reduced magnitude. This can be understood when considering that the MD swimmers interact with the spheres only for the short duration where they physically collide, while the HDMD swimmers interact with spheres on approach, during physical collision, and through the wake upon departure. The HDMD swimmers also cause an impact when they avoid a sphere and pass by the side, an interaction entirely missing with MD swimmers. Quantitatively, the value of the MSD at 25 s is 8×10^3 μm^2 for HDMD, 17 μm^2 for MD, and 16 μm^2 for a BD control (isolated sphere, $D = k_BT/\gamma$). While the HDMD case yields values comparable with the experimental results in Fig. 2 of [16], the MD case (without BD) is nearly indistinguishable from an isolated sphere experiencing thermal fluctuations.

The radial distribution function $g(r)$ between spheres

is given in Fig. 3. The only explicit interaction between spheres defined in the mechanics is a steric repulsion, and an ideal case would lead to a nearly flat $g(r)$ (outside the excluded volume region) indicating no organization (the spheres here have a packing fraction of only 0.04). Here we see a characteristic peak at d, indicating the formation of pairs and the existence of effective attraction between spheres, and a secondary peak at $1.2d$ which is the separation caused when a swimmer moves between two spheres and splits them apart. When a pair gets into a tightly bound state at d, most forces acting on the pair will either cause it to rotate or translate (preserving distance). One can imagine the bath of active matter representing a fluctuating field of forces (including both collisions and hydrodynamic effects) acting on the pair, and only a high degree of local variability (along the connecting axis) will cause the pair to split. This typically occurs due to direct physical contact from an approaching swimmer, although it is possible for swimmers moving parallel to the side of a pair to produce a field which increases the distance between the spheres (since the front and back velocity fields are in opposing directions). This reflects the work done in [19], but there is an important qualitative distinction. While the MD peak occurs strictly at $1.2d$ and to the right of it, the HDMD peak is entirely contained to the left of $1.2d$, indicating that the act of a swimmer passing between a pair of spheres causes some post-collision stabilization. We can understand this in terms of the swimmer's flow field, as given in Fig. 1. The fluid to the sides of a swimmer is entrained inward, so that a swimmer draws nearby spheres towards it if it passes between them. While this force is weak at long distances, the effects are clearly visible at short distances. This type of interaction is impossible to achieve in the (purely-steric) MD simulations. This leads to the conclusion that pair stability is enhanced by fluid dynamics (since the primary originator of pair separation is the action of a swimmer passing directly between two spheres). However, the dynamical timescales are so widely separated between MD and HDMD simulations that it is difficult to definitively make this claim. Recall that the MSD is orders of magnitude apart, so that pair lifetimes are an order of magnitude longer in MD simulations (typically 18 s for MD and 2 s for HDMD on average), but this does not mean the pairs are more stable. Still, this helps to explain a discrepancy uncovered in [19], where the (MD) simulations yielded more intermittent pair behavior as opposed to that observed in experiment. That is, when a pair experiences a potential break, the typical separation incurred is much smaller for the case with hydrodynamics, so that any simulation without hydrodynamics will see pairs break more easily. Another feature of this plot is the general reduction in magnitude for the interpeak region in MD simulations. Data for contact numbers will help to elucidate the result of this distinction.

Table I shows the likelihood of spheres to form contacts at any time (where a contact is defined by a pairwise distance less than $2d$). A variety of different pair formation cutoffs and alternative pair definitions were tested, and the results were found to be robust and insensitive to the method used. The HDMD spheres are much more likely to form pairs (20% more) and triplets (85% more). This result is echoed and clarified in Fig. 4, which shows the coordination number,

$$N(r) = \int_0^r 2\pi r' g(r') dr', \tag{6}$$

around a sphere as a function of distance. The number of spheres within w for HDMD is approximately 5 times (see inset) that seen in the MD case, indicating a significant increase in the number of tightly bound pairs. This is likely due to the effective stabilization caused by the fluid flow of an impinging swimmer, which tends to keep the pair within $1.2d$ rather than force the pair outside that distance as in the MD case. While the symmetry of the hydrodynamic field would yield both attraction and repulsion in equal amounts after a swimmer splits a pair, there is an asymmetry invoked by the reorientation of the swimmer: attractive fluid flows occur immediately after the split, but the full extent of repulsive flow will never

TABLE I. Percent likelihood of number of sphere contacts (with other spheres) for HDMD and MD simulations. Pairs and triplets are significantly more likely to form in the HDMD case, and likewise the number of lone spheres is reduced. The standard error of the mean is shown.

Contacts	MD %	HDMD %
0	70.3 ± 0.2	61.4 ± 0.5
1	26.0 ± 0.2	31.6 ± 0.3
2	3.5 ± 0.1	6.4 ± 0.2
3	0.2 ± 0.0	0.6 ± 0.1

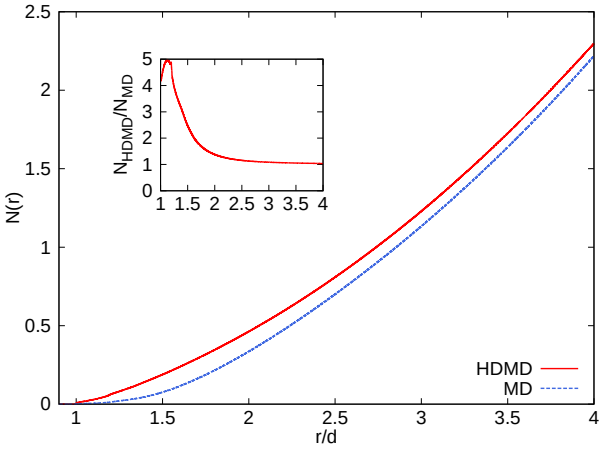

FIG. 4. (color online). Average number of spheres (coordination number) within a distance r of a given sphere (units in terms of sphere diameter d) for HDMD (red solid) and MD (blue dashed) simulations. Inset: HDMD results divided by MD results, showing significant changes close to the sphere.

TABLE II. Data as in Table I, but showing the difference between NOS/NOT and HDMD simulations (where a plus sign indicates a higher percentage for NOS/NOT). While the trend for both is an increase in contact numbers, the changes are relatively small (and in some cases statistically insignificant). The error shown is the sum of the errors for NOS/NOT and HDMD values.

Contacts	NOS △%	NOT △%
0	-2.1 ± 1.2	-3.8 ± 1.0
1	$+1.4 \pm 0.8$	$+1.7 \pm 0.8$
2	$+0.6 \pm 0.6$	$+1.8 \pm 0.6$
3	$+0.1 \pm 0.2$	$+0.3 \pm 0.2$

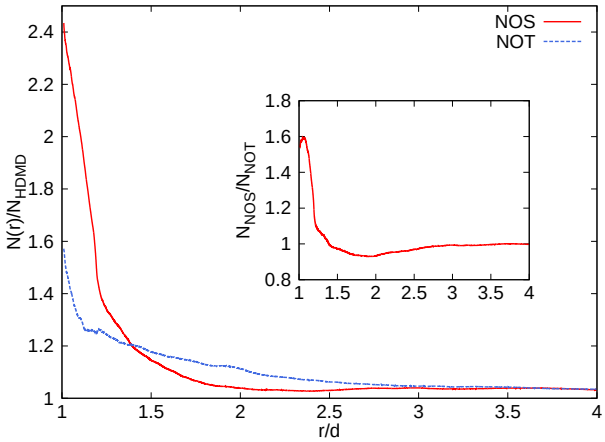

FIG. 5. (color online). NOS (red solid) and NOT (blue dashed) coordination number (see Fig. 4) divided by HDMD results. NOS lacks a g(r) peak at $1.2d$ (since no steric collision gives rise to it), which gives it a much higher coordination number at low r. NOT is higher around $2d$, signifying somewhat greater mid-range interaction between passive spheres. Inset: NOS coordination number divided by NOT results, showing the relative areas of higher and lower coordination.

occur (which would require a straight run by the swimmer over a large distance and time, without tumbling, collisions, or torque due to local variations in fluid velocity). One can also consider the fact that the quantity and duration of interactions between swimmers and passive particles is increased in the HDMD simulations (because the number of interactions is not restricted to mechanical collisions), so that the likelihood of experiencing an effective attraction at any given time is much higher. Qualitatively, the HDMD simulations contain many instances where pairs or triplets (and higher orders) move and rotate as a unit rather than as constituent individuals. This is because the fluid velocity field allows swimmers to interact simultaneously with multiple passive particles. In contrast, MD simulations are nearly incapable of exhibiting concurrent movements (at the density studied) except in cases where the spheres are in direct physical contact (which is less likely in the MD case).

In order to assess the effect that certain system elements have on the aforementioned results, two additional control simulations were performed under identical conditions to the HDMD runs, with one difference each. In the first, steric interactions between swimmers and passive spheres were removed (hereafter referred to as NOS). Steric interactions between two swimmers and between two spheres still exist, but a swimmer can only push a sphere indirectly, through its hydrodynamic field. The second simulation has no tumbling (hereafter referred to as NOT), so swimmers only reorient due to torques caused by the hydrodynamic field or direct collisions with other swimmers or spheres. While both NOS and NOT runs see an increase in contact numbers, the magnitude of these changes (seen in Table II) is relatively small. For the NOS simulation, this can be seen as the removal of the pair-splitting collision described above. Since the hydrodynamic field tends to restore the pair after this, the change is somewhat insignificant. Nevertheless, it is clear that steric collisions do not play a significant role in this system when it comes to contact numbers. The effect is somewhat more pronounced for the NOT system, and is most likely due to the overall increase in the attractive interaction between spheres. With no swimmers in the tumble phase, there are effectively more swimmers in the run phase, which means the magnitude of the fluctuating force that impacts a pair is increased. The number of tumblers in the HDMD system is ≈10% only, which explains why the increase is not too significant. This data can also be seen in a comparison of the coordination numbers of NOT, NOS, and HDMD simulations, as given in Fig. 5. While the NOS simulation naturally has a higher degree of coordination at low r, the effect diminishes quickly with increasing r. This is effectively the absence of the peak at $1.2d$ seen in HDMD/NOT simulations (since it is a direct result of steric collisions). In contrast, the NOT $N(r)$ experiences a more gradual decline toward N_{HDMD} at large r. This is a result of the range of interaction between spheres increasing as a result of the greater strength of the fluctuating field. The force acting on a pair must overcome friction in order to bring the spheres closer together; accordingly, as the driving force increases in magnitude, the range at which it can impact pair distance becomes longer. Plots of $g(r)$ for these systems have been omitted since they carry the same information but in a less easily interpreted fashion, as well as being structurally similar to the HDMD plot already given above (although without a peak at $1.2d$ for the NOS case). Fig. 6 shows the relation between the MSD of the NOT and HDMD systems. The HDMD and NOS systems are indistinguishable in this measurement, indicating that the importance of steric collisions with swimmers in the diffusion of passive spheres is minor (this is clear when looking at the magnitudes of difference in Fig. 2). In contrast, the removal of tumbling gives a noticeable increase in the MSD. The effect at short times can be seen as the increase in the driving field acting on the spheres due to a greater number of swimmers in

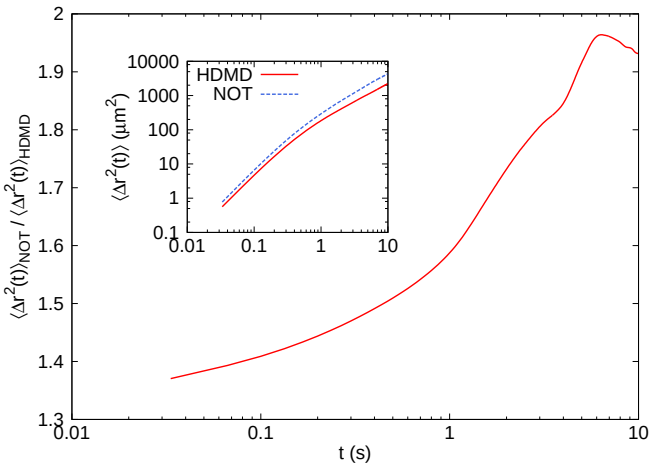

FIG. 6. (color online). Ratio of the MSD of the NOT case to the NOS/HDMD case. At short times, the absence of tumbling means a net increase in the strength of the fluctuating field (more swimmers swimming), yielding greater diffusion. The lack of tumbling also causes the system to take longer to change, thus giving a larger increase at longer times. Inset: MSD for NOS/HDMD (red solid) and NOT (blue dashed) conditions.

the run phase. Near and beyond the transition region in the MSD, the NOT system yields yet larger relative MSD, which can be seen as the effect of reduced decorrelation and reorientation of the system's constituents. At these times in the HDMD simulations, one expects more and more swimmers to have entered the tumbling phase, thus changing the direction of the forces acting on passive particles. Even without tumbling, the swimmers in the NOT simulation still reorient over time due to torques in the fluid field as well as direct collisions, so the effect does not increase forever, but rather levels out at long times. There is also the natural saturation that comes from the impact of a given swimmer diminishing with distance; i.e., even with no reorientation there would still be a limit to how long a passive sphere experiences a similar driving force. Thus while there is a quantitative difference (increase in MSD and more gradual transition between regions), the qualitative nature of the plot remains unchanged. That is to say that there is enough native reorientation (of the field acting at a particular region of space) in this system that the qualitative impact of a system having decorrelated directionality over time exists whether tumbling is included or not.

Conclusions.—We have used numerical simulations to determine the qualitative and quantitative impact of adding fluid dynamics to active-passive hybrid systems. Quantitatively, HDMD simulations exhibit dramatically higher mean squared displacements (by orders of magnitude) that yield significantly better agreement with experiment than the MD simulations. Furthermore, the relevant timescales in MD runs are reduced, and the characteristic super to simple diffusion transition is less pronounced. Additionally, HDMD spheres have a higher propensity to form contacts and these contacts appear to have a heightened stability once formed. Qualitatively, the typical pair separation procedure of a swimmer moving directly between two spheres and moving them apart by direct contact has a post-collision stabilization when fluid dynamics are added to the system, caused by the fluid velocity field around a swimmer. Pair and triplet dynamics couple more strongly in HDMD simulations, where correlated translation and rotation occurs due to the fluid field interacting with the spheres, an effect completely missing in the MD simulations. Furthermore, the importance of steric interactions between swimmers and passive spheres and swimmer reorientation by tumbling has been assessed. No qualitative difference in the results was observed for the NOT case. The system has enough reorientation through fluid torques and direct collisions to make the change merely amount to an increase in the magnitude of the driving force of the system. The absence of direct collisions in the NOS case certainly alters the radial distribution function, but both the MSD and the contact number probabilities see little change, indicating the quantitative impact of direct collisions is relatively low. While the results of this work provide clear evidence of the important impact of hydrodynamics on the effective interactions in hybrid systems, the dependence of the conclusions on system properties such as density and swimmer velocity remain poorly understood, and will be the target of future endeavors.

ACKNOWLEDGMENTS

This work was funded by the National Institutes of Health grant GM086801 and the National Science Foundation grant MCB-1050966. The authors acknowledge Dr. P. Underhill for providing insightful comments.

[1] A. Sokolov, I. S. Aranson, J. O. Kessler, and R. E. Goldstein, Phys. Rev. Lett. **98**, 158102 (2007).
[2] D. Svenšek, H. Pleiner, and H. R. Brand, Phys. Rev. Lett. **111**, 228101 (2013).
[3] J. Dunkel, S. Heidenreich, K. Drescher, H. H. Wensink, M. Bär, and R. E. Goldstein, Phys. Rev. Lett. **110**, 228102 (2013).
[4] I. S. Aranson, A. Sokolov, J. O. Kessler, and R. E. Goldstein, Phys. Rev. E **75**, 040901 (2007).
[5] A. Costanzo, R. Di Leonardo, G. Ruocco, and L. Angelani, J. Phys. Condens. Matter **24**, 065101 (2012).
[6] K. C. Leptos, J. S. Guasto, J. P. Gollub, A. I. Pesci, and R. E. Goldstein, Phys. Rev. Lett **103**, 198103 (2009).
[7] A. A. Solovev, S. Sanchez, and O. G. Schmidt, Nanoscale

5, 1284 (2013).
[8] S. Sengupta, M. E. Ibele, and A. Sen, Angew. Chem., Int. Ed. **51**, 8434 (2012).
[9] J. Gibbs and Y. Zhao, Front. Mater. Sci. **5**, 25 (2011).
[10] B. Hansen, P. J. Hansen, and T. G. Nielsen, J. Exp. Mar. Biol. Ecol. **152**, 257 (1991).
[11] K. Drescher, K. C. Leptos, I. Tuval, T. Ishikawa, T. J. Pedley, and R. E. Goldstein, Phys. Rev. Lett. **102**, 168101 (2009).
[12] R. Soto and R. Golestanian, Phys. Rev. Lett **112**, 068301 (2014).
[13] I. Buttinoni, J. Bialké, F. Kümmel, H. Löwen, C. Bechinger, and T. Speck, Phys. Rev. Lett **110**, 238301 (2013).
[14] T. Ishikawa and T. J. Pedley, Phys. Rev. Lett **100**, 088103 (2008).
[15] P. T. Underhill, J. P. Hernandez-Ortiz, and M. D. Graham, Phys. Rev. Lett **100**, 248101 (2008).
[16] X.-L. Wu and A. Libchaber, Phys. Rev. Lett **84**, 3017 (2000).
[17] C. Valeriani, M. Li, J. Novosel, J. Arlt, and D. Marenduzzo, Soft Matter **7**, 5228 (2011).
[18] D. T. N. Chen, A. W. C. Lau, L. A. Hough, M. F. Islam, M. Goulian, T. C. Lubensky, and A. G. Yodh, Phys. Rev. Lett. **99**, 148302 (2007).
[19] L. Angelani, C. Maggi, M. L. Bernardini, A. Rizzo, and R. Di Leonardo, Phys. Rev. Lett. **107**, 138302 (2011).
[20] N. Koumakis, A. Lepore, C. Maggi, and R. Di Leonardo, Nat. Commun. **4**, 2588 (2013).
[21] L. Angelani, R. Di Leonardo, and G. Ruocco, Phys. Rev. Lett. **102**, 048104 (2009).
[22] L. Angelani and R. Di Leonardo, New J. Phys. **12**, 113017 (2010).
[23] P. H. Colberg and R. Kapral, EPL **106**, 30004 (2014).
[24] L. Soler, V. Magdanz, V. M. Fomin, S. Sanchez, and O. G. Schmidt, ACSNano **7**, 9611 (2013).
[25] L. H. Cisneros, R. Cortez, C. Dombrowski, R. E. Goldstein, and J. O. Kessler, Exp. Fluids **43**, 737 (2007).
[26] D. L. Koch and G. Subramanian, Annu. Rev. Fluid Mech. **43**, 637 (2011).
[27] E. Lushi, H. Wioland, and R. E. Goldstein, Proc. Natl. Acad. Sci. U. S. A. **111**, 9733 (2014).
[28] A. Furukawa, D. Marenduzzo, and M. E. Cates, Phys. Rev. E **90**, 022303 (2014).
[29] M. E. Cates and J. Tailleur, EPL **101**, 20010 (2013).
[30] O. Pohl and H. Stark, Phys. Rev. Lett. **112**, 238303 (2014).
[31] T. Bickel, G. Zecua, and A. Würger, Phys. Rev. E **89**, 050303 (2014).
[32] S. Succi, *The Lattice Boltzmann Equation for Fluid Dynamics and Beyond* (Oxford University Press, 2001).
[33] C. S. Peskin, Acta Numerica **11**, 479 (2002).
[34] D. J. Earl, C. M. Pooley, J. F. Ryder, I. Bredberg, and J. M. Yeomans, J. Chem. Phys. **126**, 064703 (2007).
[35] R. W. Nash, R. Adhikari, J. Tailleur, and M. E. Cates, Phys. Rev. Lett. **104**, 258101 (2010).
[36] C. N. Likos, Phys. Rep. **348**, 267 (2001).
[37] H. C. Berg and D. A. Brown, Nature **239**, 500 (1972).